International Journal of Heat and Mass Transfer 52 (2009) 655–664

Contents lists available at ScienceDirect

International Journal of Heat and Mass Transfer

journal homepage: www.elsevier.com/locate/ijhmt

Low Reynolds number scalar transport enhancement in viscous and non-Newtonian fluids

D.R. Lester [a,*], M. Rudman [b], G. Metcalfe [a]

[a] CSIRO Materials Science and Engineering, P.O. Box 56, Highett, Vic. 3190, Australia
[b] CSIRO Mathematical and Information Sciences, Locked Bag 33, Clayton South, Vic. 3169, Australia

ARTICLE INFO

Article history:
Received 12 February 2008
Received in revised form 27 June 2008
Available online 18 September 2008

Keywords:
Heat and mass transfer
Chaotic advection
Parametric variation
Numerical methods

ABSTRACT

Enhancement of heat and/or mass transfer via turbulence is often not feasible for highly viscous, non-Newtonian or shear sensitive fluids. One alternative to improve transport within such materials is chaotic advection, whereby Lagrangian chaos occurs within regular (non-turbulent) flows [J.M. Ottino, The Kinematics of Mixing: Stretching, Chaos and Transport, Cambridge University Press, Cambridge, 1989]. Complex interactions between chaotic advection and diffusion yields enhanced dispersion, and the topology of the Lagrangian dynamics is governed by the set of control parameters for the flow device. What parameter set maximises scalar dispersion for a given fluid rheology and diffusivity? Most studies to date have only considered a handful of points in the parameter space $\mathcal{Q}$, but as this space may be large and the solution distribution complex (fractal), robust optimisation requires detailed global resolution of $\mathcal{Q}$. By utilising a novel spectral method [D.R. Lester, G. Metcalfe, M. Rudman, H. Blackburn, Global parametric solutions of scalar transport, J. Comput. Phys. (2007). doi: doi:10.1016/j.jcp.2007.10.015] which exploits the symmetries often present in chaotic flows, we can resolve the asymptotic transport dynamics over $\mathcal{Q}$, facilitating the identification of optima and elucidating the global structure of transport. We employ this method to optimize scalar transport for both Newtonian and non-Newtonian fluids in a chaotic mixing device, the Rotated Arc Mixer (RAM). Significant (up to sixfold) acceleration of scalar transfer is observed at Peclét number $Pe = 10^3$, which furthermore increases with Pe.

1. Introduction

1.1. Motivation

Many industrial processes require rapid transport of heat and/or mass within highly viscous or non-Newtonian materials such as emulsions, suspensions, slurries and pastes. For example, food sterilization demands uniform heating of shear sensitive or temperature sensitive foodstuffs within a narrow temperature range, and reaction of biological agents requires gentle yet rapid mixing of reagents as well as precise temperature control to inhibit undesirable side reactions.

For high viscosity fluids, diffusion and natural convection alone are generally insufficient to achieve the required heat and mass dispersion rates, so forced convection is also required. However, traditional approaches such as introduction of turbulence are often not feasible for highly viscous, non-Newtonian or shear sensitive materials due to large energy costs, complex rheology, and sometimes delicate nature of these materials. With these considerations in mind, a promising method to enhance transport characteristics of highly viscous or non-Newtonian materials is chaotic advection [12], whereby chaotic fluid particle paths arise from a velocity field which may be non-turbulent, and in some cases even completely steady. Lagrangian chaos can be achieved even within Stokes flow and so this method is attractive for processing of shear-sensitive fluids.

1.2. Background

While chaotic advection directly enhances transport of passive entities (i.e. mixing of non-diffusive tracers), these principles also apply to dissipative systems, e.g. the transport of diffusive species or heat. Due to complex interactions between kinetic advection and dynamic molecular transport processes, the fundamentals of chaotic advection–diffusion are not fully understood [4,22], however, the potential benefits of such phenomena are substantial. From a practical perspective, what is the magnitude of these benefits, and how can we exploit them?

Chaotic advection devices often involve a number of variable design and operating parameters which must be optimised for the process at hand. For non-diffusive mixing, global chaos is desirable, whereas for other applications, different protocols may be preferential. For diffusive mixing or heat transfer, the relative

* Corresponding author. Tel.: +61 3 9252 6195; fax: +61 3 9252 6240.
E-mail address: daniel.lester@csiro.au (D.R. Lester).

0017-9310/$ - see front matter Crown copyright © 2008 Published by Elsevier Ltd. All rights reserved.
doi:10.1016/j.ijheatmasstransfer.2008.06.039

timescales of advection and diffusion must be accounted for. In all but trivial flows, the optimum set of control parameters cannot be determined analytically, so experimental or numerical investigation is required. As the control parameter space (denoted $\mathcal{Q}$) can be large, and results herein suggest the transport rate has a complex (fractal) distribution, high-resolution global exploration of $\mathcal{Q}$ is required to robustly identify global optima. Until recently, the computational overhead of this operation has been prohibitive, hindering development of enhanced transport devices based upon chaotic advection. To date, most studies involving enhancement of heat transfer or diffusive mixing via chaotic advection have considered only a handful of points within $\mathcal{Q}$ [6,2,16,14]; in these cases it is unlikely the global optimum has been achieved.

Diffusive entities such as heat and mass can be active scalars, in that their distribution influences the flow field. However, very often the fluid velocity field is independent of their distribution, in which case they can be considered passive. For heat and mass transfer, such decoupling corresponds to neglecting changes in density, surface tension and viscosity with temperature and species concentration. Under such conditions, heat and mass transfer is governed by advection and diffusion, and henceforth we refer to the resultant dispersion as scalar transport. When the fluid velocity field is independent of the scalar distribution, a novel spectral method [8] is applicable which exploits the symmetries of chaotic flows, facilitating rapid and detailed global resolution of $\mathcal{Q}$. Solutions to the advection–diffusion equation (ADE) governing scalar transport are given in terms of so-called "strange eigenmodes" [9]. In the case of periodic advective velocity fields, strange eigenmodes are exponentially decaying periodic patterns. Eventually the slowest decaying strange eigenmode dominates, and so the asymptotic transport characteristics are governed by this eigenmode. As such, transport characteristics may be inferred from the dominant strange eigenmode rather than the full solution of the scalar advection equation, greatly simplifying analysis.

The aim of this work is to utilize the composite spectral method to quantify and optimize heat or mass transfer over $\mathcal{Q}$ for both Newtonian and non-Newtonian fluids within a particular flow device. As temperature homogenisation is generally of primary industrial concern for heat transfer, and insulated boundary conditions are inherent for mass transfer, to generalise we consider scalar transport here with (possibly inhomogeneous) Neumann boundary conditions. The flow device under consideration is a chaotic mixing device, the Rotated Arc Mixer (RAM) [11], which contains a number of tunable design and operating parameters, and can continually process fluids at an industrial scale. Two fluids are investigated; a high viscosity Newtonian fluid and a yield stress, shear thinning fluid. The former case quantifies transport enhancement for highly viscous but rheologically simple materials, whereas the latter relates to particularly problematic materials as the plug flow regions inherent to yield stress fluids present natural barriers to transport. To quantify transport enhancement, we compare the RAM with that for a straight tube with the same boundary conditions, and compare optimised scalar transport and energy requirements for both rheologies. This study demonstrates both applicability of the composite spectral method to industrially relevant problems, and furthermore quantifies the potential for chaotic advection to enhance heat and mass transfer within highly viscous and non-Newtonian fluids.

In the following section, the RAM geometry and control parameters are reviewed, and the relevant governing equations outlined. In Section 3 the solution method is outlined, followed by the Newtonian and non-Newtonian analyses in Sections 4 and 5, respectively. These results are summarised in Section 6 and conclusions are presented in Section 7.

2. Problem definition

2.1. RAM geometry and parameters

As a detailed description of the RAM and its operational principles are given in Metcalfe et al. [11], only a brief summary of the device and geometry is given here. A schematic of the RAM is illustrated in Figs. 1 and 2 depicting the RAM geometry, design and operating parameters. In brief, the RAM consists of an inner cylinder of inner radius R through which the fluid flows, and tightly wrapped around this is an outer cylinder which rotates at fixed angular velocity Ω. Regular apertures are cut into the inner cylinder of arc angle Δ and length L, such that at the end of one aperture (in axial direction), another is cut immediately afterwards, offset by angle Θ, resulting in a reoriented duct flow [19]. Rotation of the outer cylinder imparts a transverse flow in addition to the axial flow along the inside of the inner cylinder. Each "cell" of the RAM corresponds to an aperture, and each cell experiences a combination of these axial and transverse flows. From cell to cell, this basic flow is simply reoriented by the offset angle Θ. If U denotes the average axial velocity, then the ratio of timescales between the axial to transverse velocities is defined as

$$\beta = \frac{\Omega L}{U}. \tag{1}$$

The set of three flow control parameters β, Δ, Θ determine mixing conditions within the RAM, along with the usual rheological, inertial, and surface parameters of the fluid. Diffusion introduces a further parameter quantifying the timescale between advection and diffusion, namely the Peclét number Pe, which scales linearly with rotation rate Ω:

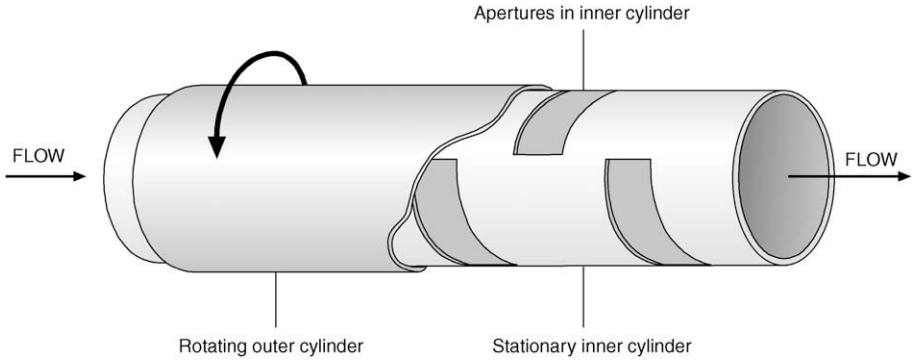

Fig. 1. Rotated Arc Mixer schematic.

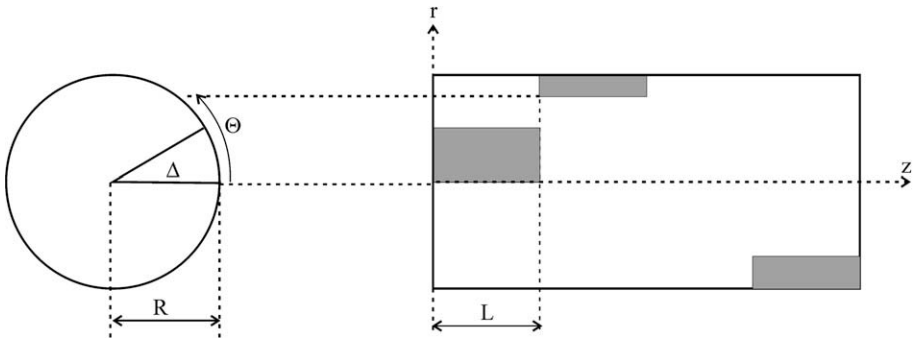

Fig. 2. Rotated Arc Mixer geometry and parameters.

$$Pe = \frac{V_0 L_0}{D_0} = \frac{\Omega R^2}{D_0}. \tag{2}$$

where D_0 is the scalar diffusivity and V_0, L_0 are the characteristic transverse velocity and length scales. This set of four control parameters $\{\beta, \Delta, \Theta, Pe\}$ govern heat and mass transfer within the RAM, and it is these parameters which may be adjusted to optimise scalar transport.

2.2. Governing equations

Metcalfe et al. [11] show experimentally that for both Newtonian and non-Newtonian (but not viscoelastic) fluids, the relative thickness of the transition region between cells with respect to the aperture length L is negligible for Reynolds numbers $Re < 50$. This does not represent a practical limitation as the RAM is designed to operate with viscous-dominated flows. In essence the so-called "two and a half dimensional" formulation [11] ignores transition flows at cell boundaries within the RAM; consequently, the flow field in each cell is considered two-dimensional. The extra "half dimension" refers to the fact that the transverse and axial flows can be coupled via the rate dependant non-Newtonian viscosity. The solution method utilized herein is quite general, and may also be applied to Hamiltonian 2D flows, time-periodic and/or spatially periodic 3D flows. Cases involving time-periodic moving boundaries are also applicable, details can be found in Lester et al. [8]. Under the 2.5D assumption, the RAM velocity field can be considered piecewise constant in z, and so the full RAM velocity field $\mathbf{u}(r,\theta,z)$ can be mapped from the velocity field in the first cell, $\mathbf{v}(r,\theta)$ as

$$\mathbf{u}(r,\theta,z) = \mathbf{v}\left(r, \theta - \Theta \sum_{k=1}^{\infty} H(z-kL)\right), \tag{3}$$

where H is the Heaviside step function. This mapping yields significant simplifications as not only does solution of the cell velocity field $\mathbf{v}$ reduce to a 2D problem, but furthermore $\mathbf{v}$ is independent of the parameters Θ and L (or β in dimensionless form). For rational values of Θ/π, the full RAM velocity field $\mathbf{u}$ is z-periodic with periodicity jL for some integer j.

For both rheologies, the steady, incompressible, non-buoyant flow is driven transversely by the rotating outer sleeve of the RAM and axially by a constant axial pressure gradient C_p, with non-slip boundary conditions throughout. The pressure field p is of the form $p = P(r,\theta) + C_p z$. The cell velocity is $\mathbf{v}$ is governed by the continuity and Navier–Stokes equations

$$\nabla \cdot \mathbf{v} = 0, \tag{4}$$

$$\rho \mathbf{v} \cdot \nabla \mathbf{v} = \nabla \cdot (2\eta\sigma) - \nabla p, \tag{5}$$

where $\sigma = \frac{1}{2}(\nabla \mathbf{v} + (\nabla \mathbf{v})^T)$ is the rate of deformation tensor, $\eta(\dot\gamma)$ the fluid viscosity, $\dot\gamma = \sqrt{2\sigma : \sigma}$ the shear rate, and ρ the fluid density. For the Newtonian fluid the viscosity η is constant, whereas for the yield stress shear thinning non-Newtonian fluid, a Herschel–Bulkley (HB) rheological model is employed, with shear yields stress τ_y, fluid consistency κ, and flow index n:

$$\eta(\dot\gamma) = \frac{\tau_y}{\dot\gamma} + \kappa \dot\gamma^{n-1}. \tag{6}$$

Denoting the fluid temperature (for heat transfer) or species concentration (for mass transfer) over the 3D RAM as $\phi(\mathbf{x})$, transport of ϕ is described by the steady ADE

$$\nabla \cdot (\mathbf{u}\phi) = D_0 \nabla^2 \phi + f(\mathbf{x}), \tag{7}$$

subject to the inlet and wall boundary conditions

$$\phi(r,\theta,0) = \phi_0(r,\theta), \tag{8}$$

$$\left.\frac{\partial \phi}{\partial r}\right|_{r=R} = g(\theta, z), \tag{9}$$

where f and g, respectively, are the domain and boundary source terms. We split the solution to (7) into fully developed $\bar\phi$ and zero mean $\tilde\phi$ solutions, such that for f, $g = 0$, $\lim_{z\to\infty} \tilde\phi \to 0$, and $\bar\phi = \langle \phi_0 \rangle$, where $\langle\ \rangle$ denotes averaging over r, θ.

As the ADE is linear, non-dimensional analysis provides significant generalisation of the results. Indeed, for a Newtonian fluid in the Stokes limit, a non-dimensional formulation is universal, whereas for the HB fluid, the analysis is general across cases where the dimensionless cell fluid velocity is constant (these cases can be found by non-dimensionalising the HB model (6) and momentum equation (5) as per Speetjens et al. [19]). Introducing the scalings $r' = r/R$, $z' = z\Omega/U$, $u'_z = u_z/U$, $\mathbf{u}'_{r,\theta} = \mathbf{u}_{r,\theta}/(\Omega R)$, $\phi' = \phi$ and substitution (upon dropping primes) of these and the continuity equation (4) gives the non-dimensional scalar transport equation (STE)

$$u_z \frac{\partial \phi}{\partial z} = -\mathbf{u}_{r,\theta} \cdot \nabla_{r,\theta} \phi + \frac{1}{Pe} \nabla^2_{r,\theta} \phi + \frac{1}{\Omega} f(\mathbf{x}), \tag{10}$$

where the axial conduction term $\frac{\partial^2 \phi}{\partial z^2}$ is ignored under assumptions that $L \sim R$ and that transverse temperature gradients dominate over axial gradients due to the transverse velocity in the RAM. Schneider [17] suggests this assumption is valid for axial Peclét numbers $Pe_{ax} = UR/D_0 > 100$, as is the case for the flows considered here. In cases where this term is significant (such as heat transfer in micro-channel flow [15]), with minor modification (extension to a nonlinear eigen problem), the spectral analysis is still applicable.

In summary, scalar transport representing heat or mass transfer in the RAM is described by the dimensionless STE (10), coupled via the RAM velocity field $\mathbf{u}$ to the mapping (3) and Navier–Stokes (4) and (5) equations. The RAM control parameters Δ, Θ, β characterize the dimensionless advective field for a given fluid, and the Peclét number Pe quantifies the relative timescale of advection and diffusion. Maximisation of scalar transport in the RAM represents an optimisation problem over this control parameter

set $\{\Delta, \Theta, \beta, Pe\}$ for a given fluid rheology. This set of design and operating parameters form a four-dimensional space which govern the scalar dispersion characteristics of the device.

Following previous investigations [11,8,19], we consider $\Delta = \pi/4$ only, as this aperture opening angle appears to be close to optimal for a wide range of fluids, however, consideration of other aperture opening angles simply represents increased computational effort. Theoretical analysis [22] and numerical results [8] indicate that the optimized transport enhancement rate increases monotonically with Pe, and so scalar transport is expected to be optimal in the limit $\Omega \to \infty$. However, as the RAM is a viscous mixing device, there exists a practical limit of $Re_{\max} \sim 50$ [11], beyond which the transverse flow achieved by the rotating outer cylinder no longer penetrates significantly into the flow cavity, and mixing is severely retarded. This corresponds to an upper limit in Peclét number of

$$Pe_{\max} = Re_{\max} Pr = Re_{\max} \frac{\nu}{D_0}, \tag{11}$$

where ν is the kinematic viscosity, and Pr is the (heat or mass) Prandtl number, a material property. To address this generality, we consider a moderate Peclét number of $Pe = 10^3$ here, which corresponds to a fairly high scalar diffusivity $D_0 = 2 \times 10^{-5}\ \mathrm{m^2\ s^{-1}}$ for species in a fluid such as water. These results herein are interpreted with the understanding that further improved scalar transport is possible at higher Pe, however, the optimal set of remaining parameters $\{\beta, \Theta\}$ may be different. As the kinematic viscosity is typically much larger for highly viscous or non-Newtonian fluids, and the scalar (heat or mass) diffusivity typically lower, a much higher $Pe_{\max}$ (and hence transport enhancement) may be achievable for such materials.

Optimisation of heat or mass transfer in the RAM for $\Delta = \pi/4$ and $Pe = 10^3$ corresponds to maximisation of scalar transport rate (governed by (10)) over the control parameter space $\mathcal{Q} : \{\beta, \Theta\} = [0, \infty) \times [-\pi, \pi]$. To perform this optimisation, a universal metric to characterise scalar transport for various scenarios, e.g. heat and/or mass transfer, inlet conditions and different possible boundary or domain sources is derived below.

3. Solution method

As the RAM cell velocity $\mathbf{v}$ is independent of both ϕ and the parameters $\{\Theta, \beta\}$, the Navier–Stokes equations need only be solved once for each fluid rheology. Subsequently the RAM velocity field $\mathbf{u}$ can be constructed via the mapping (3) for any choice of β and Θ, and solution of the STE (10) performed.

For the Newtonian fluid rheology, the RAM cell velocity field $\mathbf{v}$ is analytic, where the transverse velocity field is given by Hwu et al. [5], and the axial velocity distribution is the parabolic profile for laminar tube flow. The 2D steady Navier–Stokes equations (4) and (5) for the Herschel–Bulkley fluid are solved numerically using the commercial CFD package CFX-10, where a series of increasing refined meshes is used to establish convergence and accuracy of the solution. To ensure incompressibility is satisfied, the cell velocity in both cases is expressed as $\mathbf{v} = \hat{\mathbf{e}}_z \times \nabla \mathbf{\Psi}_{r,\theta} + v_z \hat{\mathbf{e}}_z$, where $\hat{\mathbf{e}}_z$ is the axial unit vector and $\mathbf{\Psi}_{r\theta}$ the transverse flow stream function. This formulation also facilitates computational savings when performing spectral expansion of $\mathbf{v}$ [8].

Given solution of the RAM velocity field $\mathbf{u}$, an efficient method is required to solve the scalar transport equation over $\mathcal{Q}$. Solutions of the STE (10) may be cast in terms of strange eigenmodes, which in essence are the Floquet modes of the periodic steady 3D system (the dimensionless RAM velocity is βj-periodic in z). Liu and Haller [9] have established existence and convergence of these solutions under reasonable conditions, providing a mathematical basis for decomposition of solutions of the ADE into a finite number of superimposed strange eigenmodes and an arbitrarily small fast-decaying non-eigenmode term. As such, the zero mean part of the dimensionless scalar field may be represented as

$$\tilde{\phi}(\mathbf{x}) = \sum_{k=0}^{K} \alpha_k \varphi_k(\mathbf{x})\, \mathrm{e}^{-\lambda_k x} + \mathcal{O}(\mathrm{e}^{-\rho z}), \tag{12}$$

where $\varphi_k(\mathbf{x})$ is the kth strange eigenmode (which is βj-periodic in z), λ_k is the associated decay rate, α_k is the weighting due to projection onto the initial condition $\phi_0(r,\theta)$, and the final term is the non-eigenmode contribution. Strange eigenmodes may also be complex, the pattern in which case has spatially quasiperiodic or subharmonic eigenmodes, depending upon whether $\mathrm{Im}(\lambda_k)$ is rational with respect to π/β.

3.1. Quantification of scalar transport enhancement

To derive a universal metric for scalar transport *enhancement* within the RAM, performance is compared with a reference case of simple tube flow with the same scalar boundary conditions. For each rheology, we consider the same fluid flowing with the same mean axial velocity U in a tube of the same dimensions as the RAM. As such, transport enhancement in the RAM can be correlated with the energy difference associated with driving of the transverse flow and different axial pressure gradients. For simple tube flow the scalar transport equation (10) is

$$u_z(r) \frac{\partial \phi}{\partial z} = \frac{1}{Pe} \nabla^2_{r,\theta} \phi + f(\mathbf{x}) \tag{13}$$

subject to boundary conditions (8) and (9). The axial velocity $u_z(r)$ is dependant upon the fluid rheology; this problem is well studied [18] for the Newtonian case. If $\Xi_k(r,\theta)$, $-\xi_k$, respectively, denote eigenfunctions and eigenvalues of the operator $1/u_z(r)\nabla^2_{r,\theta}$, then solutions to (13) for f, $g = 0$ are of the form

$$\tilde{\phi}(\mathbf{x}) = \sum_{k=0}^{\infty} \gamma_k \Xi_k(r,\theta)\, \mathrm{e}^{-\frac{\xi_k}{Pe} z}, \tag{14}$$

where γ_k is the projection of the zero mean initial conditions onto the kth eigenfunction. These results serve a basis for quantification of scalar transport enhancement in the RAM; we consider the following distinct cases:

- Homogenization of an initial scalar distribution with no domain or boundary sources; i.e. diffusive mixing or insulated heat transfer.
- Continual homogenization of the scalar field with a domain source; i.e. insulated heat or mass transfer with an internal heat or mass source.
- Transition to a fully developed profile for inhomogeneous boundary conditions; i.e. heat transfer with fixed heat flux at the boundary.

Any heat or mass transfer problem with prescribed (homogeneous or inhomogeneous) Neumann boundary conditions is covered by a combination of these problems, and so we wish to derive a universal metric for scalar transport enhancement for these cases.

3.1.1. Homogenization of initial conditions

For the first case, strange eigenmodes dictate the rate of decay of the initial distribution to the homogeneous state $\tilde{\phi} = 0$ (where $\tilde{\phi} = \phi - \bar{\phi} = \langle \phi_0 \rangle$). With increasing z (i.e. downstream distance), the slowest decaying eigenmode dominates, so the asymptotic system dynamics may be approximated by this eigenmode

$$\lim_{z \to \infty} \tilde{\phi}(\mathbf{x}) = \tilde{\phi}_\infty(\mathbf{x}) = \alpha_0 \varphi_0(\mathbf{x})\, \mathrm{e}^{-\lambda_0 z}. \tag{15}$$

Hence, λ_0 is the lengthscale of asymptotic decay of inhomogeneities in the scalar field ϕ. As the slowest decaying eigenmode is also the most regular [9] (i.e. lowest variance), there is a natural tendency for the majority of initial data to be projected onto this mode, so in most cases $|\alpha_0| \gtrapprox |\alpha_k|$ for all k_0. Therefore, convergence of $\tilde{\phi}$ to $\tilde{\phi}_\infty$ with z (quantified as $|\alpha_0 \mathrm{e}^{-\lambda_0 z}| \gg |\alpha_k \mathrm{e}^{-\lambda_k z}|$ for all k) is rapid, and the dominant strange eigenmode accurately quantifies transport a short distance downstream. As most industrial processes are concerned with dispersion to a near-homogeneous state, it is ultimately the lengthscale λ_0 that is of importance regardless of small-z dynamics. Similarly for the reference case of simple tube flow, the asymptotic dynamics are

$$\lim_{z\to\infty} \tilde{\phi}(\mathbf{x}) = \tilde{\phi}_\infty(\mathbf{x}) = \gamma_0 \Xi_0(r,\theta)\, \mathrm{e}^{-\frac{\xi_0 z}{Pe}}, \tag{16}$$

and so the lengthscale of asymptotic scalar decay in this case is ξ_0/Pe. Consequently, we define the scalar transport transfer enhancement factor q for the RAM as

$$q \equiv \frac{Re(\lambda_0) Pe}{\xi_0}. \tag{17}$$

In practical terms, in the asymptotic limit a tube with Neumann boundary conditions needs to be q times longer to achieve the same degree of scalar homogenization as the RAM.

3.1.2. Homogenization of domain sources

For the case of domain sources terms (i.e. heat, mass sources) with zero initial conditions and insulated boundary conditions, the scalar distribution ϕ can be split into average $\bar{\phi}$ and zero mean $\tilde{\phi}$ (where $\langle u_z \tilde{\phi} \rangle = 0$) contributions, where

$$\bar{\phi} = \int_0^z \left\langle \frac{f(\mathbf{x})}{u_z} \right\rangle \mathrm{d}z, \quad \tilde{f}(\mathbf{x}) = f(\mathbf{x}) - u_z \left\langle \frac{f(\mathbf{x})}{u_z} \right\rangle, \tag{18}$$

and

$$\begin{aligned} u_z \frac{\partial \tilde{\phi}}{\partial z} &= -\mathbf{u}_{r,\theta} \cdot \nabla_{r,\theta} \tilde{\phi} + \frac{1}{Pe} \nabla^2_{r,\theta} \tilde{\phi} + \tilde{f}(\mathbf{x}), \\ \left.\frac{\partial \tilde{\phi}}{\partial r}\right|_{r=1} &= 0, \tilde{\phi}(r,\theta,0) = 0. \end{aligned} \tag{19}$$

In this case the RAM acts to homogenise the scalar field ϕ, and so $\tilde{\phi}$ quantifies the scalar transport rate. The evolution of $\tilde{\phi}$ in (19) is again dictated by strange eigenmodes, which are continually excited by the zero mean source $\tilde{f}$:

$$\tilde{\phi}(\mathbf{x}) = \sum_{k=0}^{K} \left(\int_0^z F_k(u)\, \mathrm{e}^{\lambda_k u}\, \mathrm{d}u \right) \varphi_k(\mathbf{x})\, \mathrm{e}^{-\lambda_k z}, \tag{20}$$

where

$$\frac{\tilde{f}(\mathbf{x})}{u_z} = \sum_{k=0}^{K} F_k(z) \varphi_k(\mathbf{x}). \tag{21}$$

Note that if $\tilde{f}$ is constant in z, $F_k(z)$ has the same periodicity as φ_k, and if $\tilde{f}$ is bounded, $F_k(z)$ is likewise. Eq. (20) can be expressed as

$$\tilde{\phi}(\mathbf{x}) = \sum_{k=0}^{K} \sum_{n=0}^{\infty} \frac{(-1)^n}{\lambda_k^{n+1}} \left[F_k^{(n)}(z) - F_k^{(n)}(0)\, \mathrm{e}^{-\lambda_k z} \right] \varphi_k(\mathbf{x}), \tag{22}$$

where the superscript (n) denotes the nth derivative. The left hand term in the square brackets above represents a long-z solution, and the right hand term represents a developing solution. Similar to the initial conditions in (15), more of the source term $\tilde{f}$ is projected onto the most regular (slowest decaying) eigenmodes, and so again there is a tendency for $|F_0^{(n)}(z)| \gtrapprox |F_k^{(n)}(z)|$ for all k_0 and n. Furthermore, as $\lambda_0 > \lambda_k$ also, both the developing and long-z solutions are dominated by contributions from the dominant eigenmode ($k = 0$). The long-z solution persists for non-vanishing $\tilde{f}(\mathbf{x})$, and is approximated as

$$\lim_{z\to\infty} \tilde{\phi}(\mathbf{x}) = \tilde{\phi}_\infty(\mathbf{x}) \approx \sum_{n=0}^{\infty} \frac{(-1)^n}{\lambda_0^{n+1}} F_0^{(n)}(z) \varphi_0(\mathbf{x}). \tag{23}$$

Therefore, the magnitude of persistent inhomogeneities in $\tilde{\phi}_\infty$ scale at minimum linearly with $1/\lambda_0$, and also the lengthscale of exponential decay to this state is dominated by λ_0.

For the reference case, the average $\bar{\phi}$ contribution is the same as for the RAM, whereas the zero mean $\tilde{\phi}$ contribution is

$$\begin{aligned} \tilde{\phi}(\mathbf{x}) &= \sum_{k=0}^{\infty} \left(\int_0^z G_k(u)\, \mathrm{e}^{\frac{\xi_k}{Pe} u}\, \mathrm{d}u \right) \Xi_k(r,\theta)\, \mathrm{e}^{-\frac{\xi_k z}{Pe}}, \\ &= \sum_{k=0}^{K} \sum_{n=0}^{\infty} (-1)^n \left(\frac{Pe}{\xi_k} \right)^{n+1} \left[G_k^{(n)}(z) - G_k^{(n)}(0)\, \mathrm{e}^{-\frac{\xi_k z}{Pe}} \right] \Xi_k(r,\theta), \end{aligned} \tag{24}$$

where

$$\frac{\tilde{f}(\mathbf{x})}{u_z} = \sum_{k=0}^{K} G_k(z) \Xi_k(r,\theta). \tag{25}$$

For this case the magnitude of persistent inhomogeneities in $\tilde{\phi}_\infty$ scale at minimum linearly with Pe/ξ_0, and also the lengthscale of exponential decay to this state is dominated by ξ_0/Pe, so again relative scalar transport enhancement is characterised by q (17).

3.1.3. Scalar flux through domain boundary

In the case of heat transfer with fixed heat flux boundary and zero initial conditions, it is necessary to split the temperature distribution ϕ into fully developed $\bar{\phi}(r,z)$ and developing $\tilde{\phi}(r,\theta,z)$ solutions as

$$u_z \frac{\partial \bar{\phi}}{\partial z} = \frac{1}{r} \frac{\partial}{\partial r} \left(r \frac{\partial \bar{\phi}}{\partial r} \right), \quad \left.\frac{\partial \bar{\phi}}{\partial r}\right|_{r=1} = g, \tag{26}$$

$$\begin{aligned} u_z \frac{\partial \tilde{\phi}}{\partial z} &= -\mathbf{u}_{r,\theta} \cdot \nabla_{r,\theta} \tilde{\phi} + \frac{1}{Pe} \nabla^2_{r,\theta} \tilde{\phi} - \mathbf{u}_{r,\theta} \cdot \nabla_{r,\theta} \bar{\phi}, \\ \left.\frac{\partial \tilde{\phi}}{\partial r}\right|_{r=1} &= 0, \tilde{\phi}(r,\theta,0) = -\bar{\phi}(r,0), \end{aligned} \tag{27}$$

where $-\mathbf{u}_{r,\theta} \cdot \nabla_{r,\theta} \bar{\phi}$ represents a zero mean source for $\tilde{\phi}$. For Newtonian fluids, the developed solution $\bar{\phi}$ is the same as for straight tube flow (as u_z is the same)

$$\bar{\phi}(r,z) = g\left(r^2 - \frac{r^4}{4} + 2z - \frac{7}{24} \right). \tag{28}$$

At large z the bulk $\tilde{\phi}_\mathrm{b} \equiv \langle u_z \tilde{\phi} \rangle$ and average wall developing temperatures $\tilde{\phi}_\mathrm{w} \equiv \langle \tilde{\phi}|_{r=1} \rangle_\theta$ are zero, and so for a Newtonian fluid the classic fully developed Nusselt number Nu_∞ for tube flow is recovered

$$Nu_\infty = \lim_{z\to\infty} \frac{2g}{\phi_\mathrm{w} - \phi_\mathrm{b}} = \frac{2g}{\bar{\phi}_\mathrm{w} - \bar{\phi}_\mathrm{b}} = \frac{48}{11}. \tag{29}$$

For any rheology, $\tilde{\phi}$ comprises of the decaying initial conditions (projected onto α_k), as well as the continual excitation of the eigenmodes via the source term (projected onto F_k)

$$\tilde{\phi}(\mathbf{x}) = \sum_{k=0}^{K} \left(\alpha_k + \int_0^z F_k(u)\, \mathrm{e}^{\lambda_k u}\, \mathrm{d}u \right) \varphi_k(\mathbf{x})\, \mathrm{e}^{-\lambda_k z}, \tag{30}$$

and so convergence of the Nusselt number can be determined by substitution of $\tilde{\phi}$

$$\frac{1}{Nu(z)} - \frac{1}{Nu_\infty} = \frac{\tilde{\phi}_\mathrm{w} - \tilde{\phi}_\mathrm{b}}{2g} = \sum_{k=0}^{K} A_k(z)\, \mathrm{e}^{-\lambda_k z}, \tag{31}$$

where $A_k(z)$ is a periodic function and hence bounded. Again, the lengthscale of convergence to Nu_∞ is dominated by λ_0.

For the reference case, the developing solution is of the same form as Eq. (14), where now the initial conditions are the same as those for Eq. (27). Convergence of the Nusselt number for this case is then given by the classic solution [18]

$$\frac{1}{Nu(z)}-\frac{1}{Nu_\infty}=\frac{\tilde{\phi}_w-\tilde{\phi}_b}{2g}=\frac{1}{4\pi g}\sum_{k=0}^{K}\gamma_k\int_{-\pi}^{\pi}\Xi_k(1,\theta)\,d\theta\,e^{-\frac{\xi_k}{Pe}z}, \tag{32}$$

so the lengthscale of convergence is dominated by ξ_0/Pe.

In all of these cases, to leading order the dominant eigenvalue λ_0 quantifies the rate of scalar transport in the RAM. For specific cases, the full spectrum λ_k (and associated projections onto φ_k) captures the exact scalar transport rate, however, as there is a tendency for most initial and source (both boundary and domain) data to be projected onto the dominant eigenmode $\varphi_0(\mathbf{x})$, λ_0 serves as a universal metric for scalar transport which is near exact in the limit of large z, and dominant for small z. Likewise for the reference case of simple tube flow, ξ_0/Pe quantifies scalar transport in all cases to leading order, and so the enhancement factor q serves as a natural universal metric for quantifying transport enhancement in the RAM. As such, optimisation of scalar transport in the RAM can be performed with respect to q, and a method to resolve the distribution of q over $\mathcal{D}$ is outlined below.

3.2. Composite spectral method

The composite spectral method [8] rapidly calculates the strange eigenmodes of the unsteady advection diffusion equation with time-periodic advective velocity. With minor modification, this method can also be applied to the steady ADE (10) with an axially periodic advective velocity field. In essence, the axial coordinate z replaces time, and the formulations would be identical if the axial velocity u_z were plug flow. Following Lester et al. [8], spectral expansion and truncation of (10) in terms of transverse (r,θ) Laplacian eigenfunctions with Neumann boundary conditions results in a linear ODE system for the vector $\mathbf{\Phi}(z)$ of spectral coefficients

$$\mathbf{B}(z)\frac{d\mathbf{\Phi}}{dz}=\left(\mathbf{H}(z)-\frac{1}{Pe}\mathbf{D}\right)\mathbf{\Phi}, \tag{33}$$

where $\mathbf{B}(z)$ is the axial advection operator u_z, $\mathbf{H}(z)$ is the transverse advection operator $-\mathbf{u}_{r,\theta}\cdot\nabla_{r,\theta}$, and $\mathbf{D}$ is the transverse diffusion operator $\nabla^2_{r,\theta}$. Due to the cell-wise nature of the RAM model (as reflected in the mapping (3)), $\mathbf{B}(z)$ and $\mathbf{H}(z)$ are both piecewise constant in z, and the system may be cast as

$$\frac{d\mathbf{\Phi}}{dz}=\mathbf{B}(z)^{-1}\left(\mathbf{H}(z)-\frac{1}{Pe}\mathbf{D}\right)\mathbf{\Phi}=\mathbf{A}(z)\mathbf{\Phi}. \tag{34}$$

The spectral advection–diffusion operator $\mathbf{A}(z)$ is also piecewise constant, consisting of a reorientation by angle Θ every dimensionless length $\beta:\mathbf{A}(z+\beta)=\mathbf{R}_\Theta\cdot\mathbf{A}(z)$, where $\mathbf{R}_\theta$ is the operator associated with a rotation of angle θ. Solutions to the spectral system (moving with the aperture window as a frame of reference) are of the form $\mathbf{\Phi}(z)=\mathbf{S}(z)\cdot\mathbf{\Phi}(0)$, where the solution matrix is

$$\mathbf{S}(i\beta)=\mathbf{M}_{\beta,\Theta}\cdot\mathbf{S}((i-1)\beta),\quad \mathbf{S}(0)=\mathbf{I}, \tag{35}$$

and

$$\mathbf{M}_{\beta,\Theta}=\mathbf{R}_\Theta^{-1}\cdot\exp(\beta\mathbf{A}(0)). \tag{36}$$

Due to the symmetry of repeat applications of $\mathbf{M}_{\beta,\Theta}$, the dominant strange eigenmode φ_0 and decay rate λ_0 for any values of β and Θ are given by the dominant eigenvectors and eigenvalues of $\mathbf{M}_{\beta,\Theta}$. As such, resolution of the asymptotic scalar transport rate over $\mathcal{D}$ corresponds to construction of $\mathbf{M}_{\beta,\Theta}$ via (36) and solution of the dominant eigenvectors and eigenvalues for all values of β and Θ under consideration. Efficient methods to achieve this are detailed in [8].

For non-Newtonian fluids, potential asymmetry of the axial velocity profile in the RAM results in violation of continuity (4) when rotated cells are joined during mapping (3) of the full RAM velocity $\mathbf{u}$ from the cell velocity $\mathbf{v}$. To address this problem, the transition flows at cell interfaces are approximated by determining the 3D transition flow $\mathbf{v}_{tr}(\mathbf{x})$ from a RAM cell to a regular tube to a distance z_{tr} downstream where the velocity is negligibly different from the symmetric tube solution $v_z=v_r(r)$, $\mathbf{v}_{r,\theta}=0$. Conceptually, this flow and its z-reflection are welded to each end of the RAM cell velocity $\mathbf{v}$, so the resultant flow is axisymmetric at each end

$$\begin{cases}\mathbf{v}_{tr}(r,\theta,z_{tr}-z), & 0\leqslant z<z_{tr},\\ \mathbf{v}(r,\theta), & z_{tr}\leqslant z<\beta+z_{tr},\\ \mathbf{v}_{tr}(r,\theta,z-z_{tr}-\beta), & \beta+z_t r\leqslant z<\beta+2z_{tr},\end{cases} \tag{37}$$

and so may be rotated and joined for all Θ, β as per (3) without violation of continuity. By "switching off" diffusion in the transition regions, z_{tr} can be made infinitesimally small without affecting scalar transport, reflecting experimental observations [11] that the transition region is negligibly small for such flows. Although this composition only approximates the actual transition flow between cells (which is Θ dependent) in the RAM, such flows exhibit similar characteristics, i.e. rapid transition to an axisymmetric state then transition to the asymmetric state in the proceeding cell [11].

In terms of computation, all that is required is the spectral advection operator $\mathbf{S}_{tr}$ which transforms the asymmetric RAM cell velocity to symmetric tube flow, and only needs to be calculated once. Spectrally expanding the advection operator for the transition flow $(-\mathbf{v}^{tr}_{r,\theta}/v^{tr}_z)\cdot\nabla_{r,\theta}$ as $\mathbf{A}_{tr}(z)$, $\mathbf{S}_{tr}$ is approximated as the first term of the Magnus expansion [10] which may be simplified as

$$\mathbf{S}_{tr}\approx\exp\left(\int_0^{z_{tr}}\mathbf{A}_{tr}(z)\,dz\right)=\exp(f_{tr}), \tag{38}$$

where $\mathbf{f}_{tr}$ is the spectral expansion of $-\left(\int_0^{z_{tr}}\mathbf{v}^{tr}_{r,\theta}/v^{tr}_z\,dz\right)\cdot\nabla_{r,\theta}$. Solution of the dominant strange eigenmode φ_0 and decay rate λ_0 proceeds as above, where $\mathbf{M}_{\beta,\Theta}$ is now

$$\mathbf{M}_{\beta,\Theta}=\mathbf{R}_\Theta^{-1}\cdot\mathbf{S}_{tr}^{-1}\cdot\exp(\beta\mathbf{A}(0))\cdot\mathbf{S}_{tr}. \tag{39}$$

4. Newtonian analysis

As the non-dimensional formulation for a Newtonian fluid in the Stokes regime is completely general, prescription of dimensional quantities (required for calculation of energy requirements) is deferred until Section 6. In the limit $Re\to 0$, the transverse cell velocity is analytic, as per Hwu et al. [5] (streamlines are illustrated in Fig. 3), and the dimensionless axial velocity profile is parabolic; $u_z(r)=2(1-r^2)$. We first consider the reference case of scalar transport in a tube (13) with homogeneous Neumann boundary

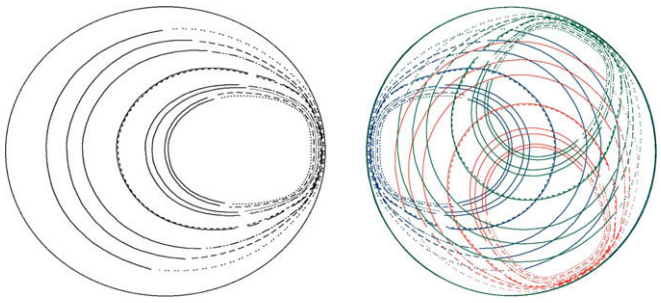

Fig. 3. RAM cell transverse flow streamlines (left) and superimposed streamlines (right).

conditions. Ignoring axial diffusion, the eigenfunctions of the advection diffusion operator $\nabla^2_{r,\theta}/u_z(r)$ are

$$\Xi_k(r,\theta) = \mathrm{e}^{\frac{-\xi_{m,n}r^2}{2}} \mathscr{L}^n_{\frac{1}{4}(-2-2n+\xi_{m,n})}(\xi_{m,n}r^2) \begin{cases} \cos(n\theta), \\ \sin(n\theta), \end{cases} \tag{40}$$

where $\mathscr{L}$ is the generalised Laguerre polynomial, $n = 0,1,2,\ldots$, and $\xi_{m,n}$ are eigenvalues of the operator. Here the dominant eigenvalue depends on whether asymmetric solutions are considered. Siegel et al. [18] considered the axisymmetric ($n = 0$) case, and found the dominant eigenvalue to be $\xi_{0,0} = 12.840$, however, there also exists a more slowly decaying eigenvalue $\xi_{0,1} = 4.161$ for the asymmetric case. The choice as to which eigenvalue to use as a reference is application dependant; $\xi_{0,0}$ is relevant to problems such as heating of a fluid with initially uniform temperature and constant wall heat flux, whereas $\xi_{0,1}$ is relevant to homogenisation of a fluid with an asymmetric initial conditions and insulated boundaries, such as diffusive mixing. We choose the axisymmetric eigenvalue as the worst case scenario, and so it is possible to *retard* scalar transport in the RAM by transferring scalar variance from axisymmetric initial conditions to a slower decaying asymmetric eigenmode. A lower bound for q is given by $\xi_{0,0}/\xi_{0,1} = 0.324$.

The dominant strange eigenmode $\varphi_0(\mathbf{x})$ and associated decay rate λ_0 for the Newtonian case is determined using the spectral method of Lester et al. [7,8] over the parameter space $\mathscr{Q} : \{\Theta, \beta\} = [-\pi, \pi] \times [0.01, 1000]$, at $Pe = 10^3$, with q calculated and plotted in Fig. 4. This plot has around 1.7×10^5 points (where the dominant strange eigenmode and associated decay rate are determined at each point), and the total computation required 2.76×10^5 s on an Intel® Xeon 3.00 GHz CPU. In contrast, using the same processor, numerical solution of the ADE only for a single point in Q to similar accuracy (to verify results of the spectral solution) using the CFD software CFX 10.0 for z large enough to observe λ_0 requires 2.3×10^5 s of computation. As such the spectral method is around 14,000 times faster to compute the global solution of Fig. 4; it is this computational efficiency which facilitates detailed exploration of the RAM control parameter space.

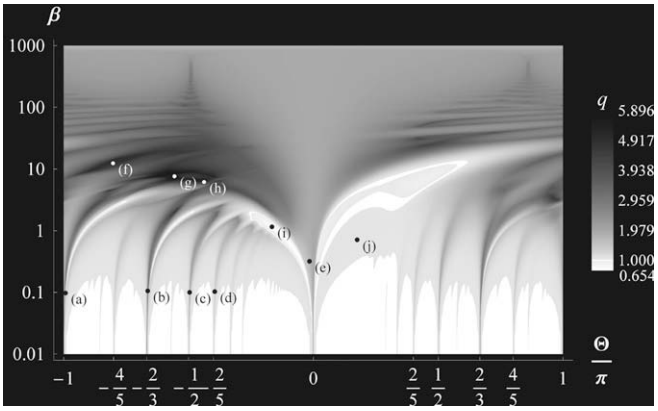

Fig. 4. Scalar transport enhancement q for Newtonian fluid in the RAM at $Pe = 10^3$.

The scalar transport enhancement distribution in Fig. 4 is of similar complex (fractal) structure to that of a Newtonian fluid in a 2D RAM with Neumann boundary conditions [7]. The eigenmodes at selected points within $\mathscr{Q}$ are shown in Fig. 5. The white region corresponds to that of negligible enhancement ($q \sim 1$), and some regions of transport retardation are observed (e.g. point (i)), associated with some transfer of variance to the slower decaying asymmetric harmonic ($\xi_{0,1}$); note that the lower bound of $q \approx 0.324$ is not reached. Ridges of transport enhancement are observed emanating from the $\beta = 0$ axis at rational values of Θ/π, with the strength of the tongues decreasing with the denominator k for $\Theta = 2\pi j/k$. Prior to collision of the ridges around $\beta = 5$, the strange eigenmodes on these ridges are ordered and rotationally symmetric as depicted in Fig. 5(a)–(d). The large gradients maintained in the programmed eigenmodes result in enhanced transport; however, off the ridges the eigenmodes are axisymmetric (e.g. Fig. 5(j)), and so scalar transport enhancement is negligible ($q \sim 1$). Enhancement also occurs in the case of no reorientation ($\Theta = 0$, Fig. 5(e)), but not to the same degree as in the dominant ridges. An order/disorder transition occurs around $\beta > 5$, resulting in greater transport enhancement in some locations (e.g. (f), (g), and (h)) than the ordered solutions. These points correspond approximately to the region of good mixing for Newtonian fluids in the RAM in the advection only case [11], where the Lagrangian dynamics are globally chaotic. There exist several regions of locally optimal enhancement within $\mathscr{Q}$ which are large enough to be considered parametrically robust. As such, transport enhancement in these regions is resistent to small perturbations arising from manufacturing imperfections, operational fluctuations, and inaccuracies in control and monitoring devices.

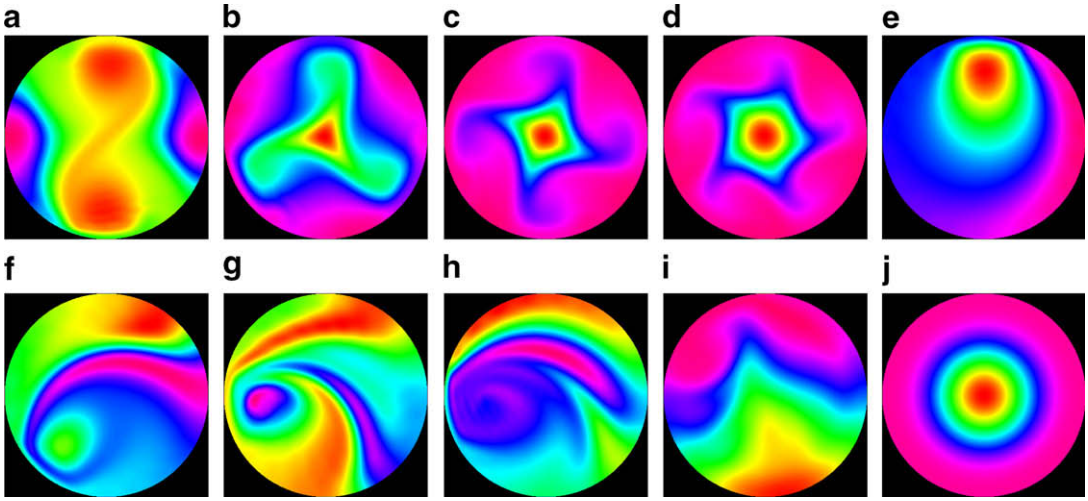

Fig. 5. Strange eigenmodes within RAM for Newtonian fluid. (a)–(c) Symmetric eigenmodes on Arnol'd tongues at $\beta = 0.2$, (d) and (e) non-symmetric eigenmodes at $\beta = 0.2$, (f)–(g) disordered eigenmodes over $\mathscr{Q}$, (i) retarded scalar transport, and (j) axisymmetric eigenmode.

The global optimum over $\mathcal{Q}$ occurs at point (g) (Fig. 4), where the scalar transport is enhanced almost sixfold ($q_{\max} = 5.814$) over the reference case. This significant enhancement means that a RAM over 5.8 times shorter than a simple tube of equivalent diameter is required to achieve the same scalar homogenisation of initial temperature or species concentration distributions for insulated boundary conditions, or transition to fully developed temperature profile for the constant heat flux problem. It is clear from Fig. 4 that detailed exploration of $\mathcal{Q}$ is critical to the optimization process and it is expected that most rapid optimization methods will fail in this complex topography. As topographical complexity over the control parameter space is ubiquitous for many dissipative chaotic systems [3], such characteristics are anticipated for all transport enhancement devices which rely upon chaotic advection.

5. Non-Newtonian analysis

To determine the specific cell velocity **v** for the non-Newtonian fluid, we consider a Herschel–Bulkley fluid with density $\rho = 1000\ \mathrm{kg\,m^{-3}}$, yield stress of $\tau_y = 20$ Pa, consistency $\kappa = 20\ \mathrm{Pa\,s^{0.5}}$, flow index $n = 0.5$ flowing within a RAM of radius $R = 0.05$ m window opening $\Delta = \pi/4$, outer sleeve rotation rate $\Omega = 1$ Hz, with axial pressure gradient $C_p = 2000\ \mathrm{Pa\,m^{-1}}$. As such, the results herein can be generalized across cases where the dimensionless cell velocity is the same, as per the scalings of Speetjens et al. [19]. CFD results for the Herschel–Bulkley RAM cell velocity (5) are shown in Fig. 6. The cell window is centered at the 3 o'clock position, where the transverse velocity is maximum. At the cell centre and the centre of the circulation region the local shear rate is zero (Fig. 6(c)) and no local transport enhancement occurs here. However, the angular offset Θ between cells means that fluid elements may experience shear in subsequent cells. These results form the basis for construction of the full RAM velocity field **u**, parameterised by β and Θ. Coupling of the axial and transverse flows via the non-Newtonian viscosity is apparent in Fig. 6(b), where the angular asymmetry arises from shear thinning of the fluid near the aperture window.

From the CFD calculations, the average axial velocity for the RAM cell is $U = 0.02116\ \mathrm{m\,s^{-1}}$. A pressure gradient of $C_p = 2137.18\ \mathrm{Pa\,m^{-1}}$ is required to achieve the same U for the non-Newtonian fluid under regular tube flow, where the axial velocity $v_z(r)$ is

$$v_z(r) = \begin{cases} \frac{(C_p R - 2\tau_y)^3}{12 C_p \kappa^2}, & 0 \leqslant r < \frac{2\tau_y}{C_p}, \\ (R-r)\frac{\tau_y^2}{\kappa^2} - (R^2 - r^2)\frac{\tau_y C_p}{2\kappa^2} + (R^3 - r^3)\frac{C_p^3}{12\kappa^2}, & \frac{2\tau_y}{C_p} \leqslant r \leqslant R. \end{cases} \tag{41}$$

As for the Newtonian case, this velocity profile is used to determine the lengthscale of asymptotic scalar transport for the non-Newtonian fluid in the reference case of tube flow. As analytic eigenfunctions of the operator $\nabla^2/u_r(z)$ are unknown, these are calculated by spectral analysis in the r-coordinate only as the dominant axisymmetric eigenfunction is used as a reference. The dominant axisymmetric eigenvalue is $\xi_{0,0} = 14.334$, and scalar transport enhancement of the RAM for the non-Newtonian case is again quantified as per (17).

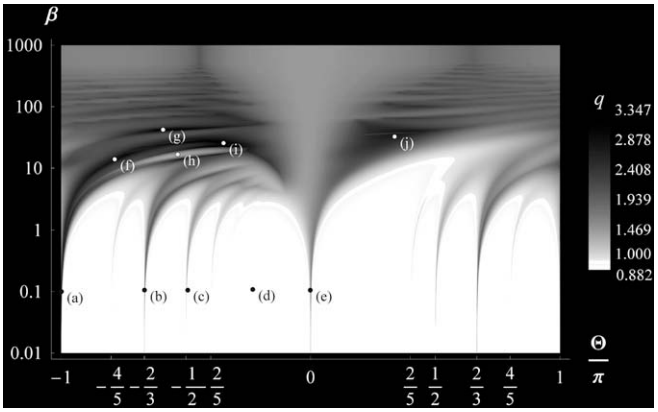

Fig. 7. Scalar transport enhancement q for the Herschel–Bulkley fluid in the RAM at $Pe = 10^3$.

The dominant strange eigenmode $\varphi_0(\mathbf{x})$ and associated decay rate λ_0 for the non-Newtonian case is determined over $\mathcal{Q}$ at $Pe = 10^3$ at similar computational expense as the Newtonian case. Once calculated, the additional overhead of including $\mathbf{S}_{\mathrm{tr}}$ in (39) is negligible. Distribution of q over $\mathcal{Q}$ is depicted in Fig. 7, and many of the qualitative features (localised ridges, order/disorder transition, localised optima) are similar to that of the Newtonian case (Fig. 4). However, the eigenmodes are now asymmetric at low β off the ridges (Fig. 8(d)) resulting in transport retardation ($q = 0.882$).

As the axial velocities between the RAM and reference cases are different, the contour $q = 1$ has no particular physical significance aside from demarcating the threshold beyond which the RAM begins to enhance scalar transport. Some transport enhancement occurs for the rotationally symmetric eigenmodes (Fig. 8(a)–(c)) on the ridges, but again optimal transport occurs in the disordered region, where more striated eigenmodes (Fig. 8(f)–(j)) occur, some of which are quasi-periodic. In contrast to the ordered solutions (Fig. 8(d) and (e)), the patterns associated with these local optima ((f), (g), and (i)) do not exhibit evidence of transport barriers associated with the plug flow region (Fig. 6(c)) of the HB fluid. As such, appropriate cell reorientation in the RAM flow is capable of transporting fluid elements (and hence ϕ) out of this region. The main point of interest in Fig. 7 is (i), where scalar transport is enhanced more than threefold ($q_{\max} = 3.347$) over the reference case of the same fluid flowing in the same geometry.

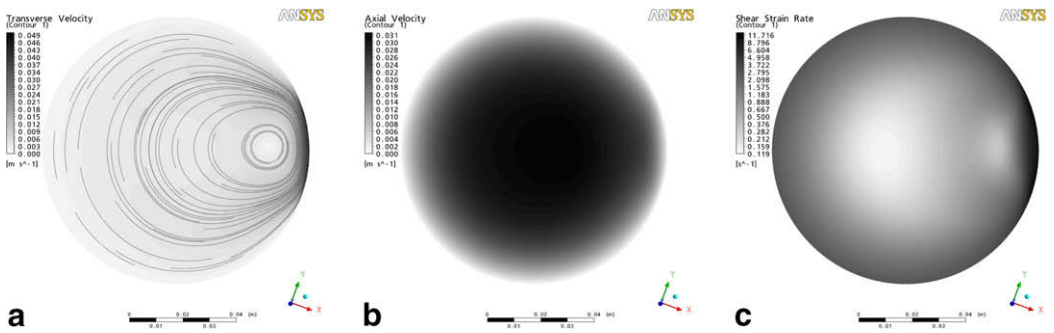

Fig. 6. RAM cell (a) transverse velocity distribution and streamlines, (b) axial velocity distribution, and (c) shear strain rate for non-Newtonian fluid within RAM cell.

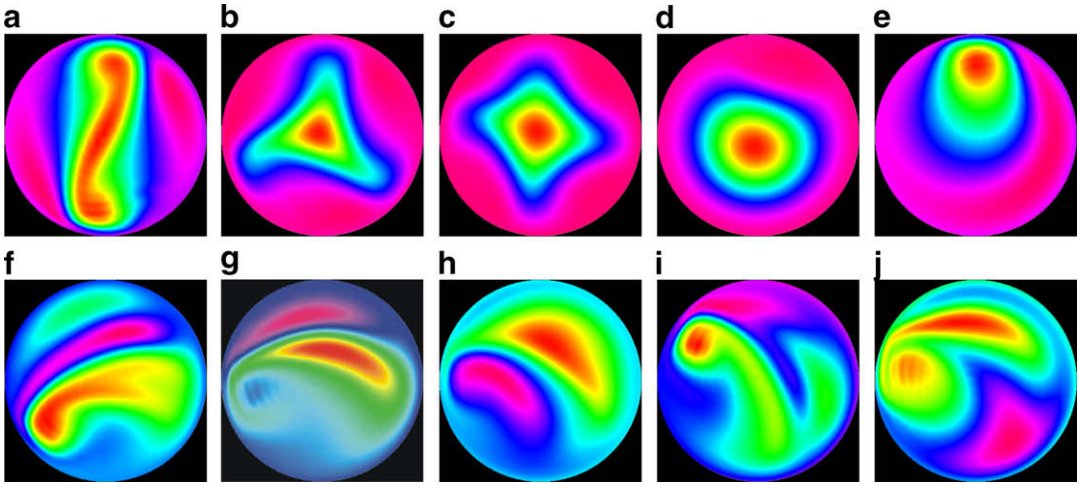

Fig. 8. Strange eigenmodes within RAM for Herschel–Bulkley fluid. (a)–(c) Symmetric eigenmodes on Arnol'd tongues at $\beta = 0.2$, (d) and (e) non-symmetric eigenmodes at $\beta = 0.2$, (f)–(j) disordered eigenmodes over $\mathcal{D}$, and (i) corresponds to optimum scalar transport.

6. Results and discussion

To determine both the cost and magnitude of scalar transport enhancement in the RAM, the energy requirements of each device for each fluid rheology must also be considered. These are calculated for the non-Newtonian fluid rheology and RAM geometry outlined in the previous Section. From the CFD results, the power per unit length required to drive the outer sleeve of the RAM for the non-Newtonian fluid is $P_{tr} = 0.1616\ \mathrm{W\,m^{-1}}$, which in addition to the axial work $P_{ax} = 0.3324\ \mathrm{W\,m^{-1}}$ gives a total of $P_{tot} = 0.4940\ \mathrm{W\,m^{-1}}$. In comparison, axial power per unit length for the same fluid at the same U in the tube is $P_{ax} = 0.3552\ \mathrm{W\,m^{-1}}$, so the RAM flow requires roughly 40% greater energy input. The shear thinning nature of the Herschel–Bulkley fluid means that the transverse work done by the rotating outer sleeve reduces the axial work; this phenomenon is common as most pseudo-plastic fluids are shear thinning.

To provide a direct comparison between the RAM flow and reference case for each rheology, we choose the Newtonian fluid viscosity to be that such that U and C_p match in the straight tube for both fluids. The mean axial velocity U for the non-Newtonian fluid (in both the RAM and tube) is $0.02166\ \mathrm{m\,s^{-1}}$, and an axial pressure gradient of $C_p = 2137.18\ \mathrm{Pa\,s^{-1}}$ in the tube is required to achieve this velocity. From the Hagen-Poiseuille law, the Newtonian fluid viscosity required to match U and C_p is $\eta = 31.563$ Pa s. This high value demonstrates applicability of the RAM to process high viscosity fluids and justifies analysis in the Stokes regime ($Re = 0.0866$). From η, the power per unit length to drive the axial flow (for both the RAM and tube flow) is calculated as $P_{ax} = \pi R^2 C_p U = 0.3552\ \mathrm{W\,m^{-1}}$. An upper bound [11] for the power consumption for the additional transverse flow in the RAM is $P_{tr} = \eta\Omega R^2 \Delta = 0.0619\ \mathrm{W\,m^{-1}}$, giving a total of $P_{tot} = 0.4172\ \mathrm{W\,m^{-1}}$.

Table 1
Scalar transport enhancement and energy requirements for straight tube and RAM processing Newtonian and non-Newtonian fluids

Rheology	Newtonian		Non-Newtonian	
Device	Tube	RAM	Tube	RAM
$U\ (\mathrm{m\,s^{-1}})$	0.02116	0.02116	0.02116	0.02116
$C_p\ (\mathrm{Pa\,m^{-1}})$	2137.18	2137.18	2137.18	2000
$P_{tot}\ (\mathrm{W\,m^{-1}})$	0.3552	0.4172	0.3552	0.4940
P_{rel}	+17.5%		+39.1%	
q_{max}	5.814		3.347	
P_{ref}	−79.9%		−58.4%	

The mean velocity U, axial pressure gradient C_p, and total power consumption per unit length P_{tot} in both the tube and RAM under each fluid rheology are summarised in Table 1. Defining P_{rel} as the relative power consumption of the RAM per unit length as compared to the straight tube, it is clear that energy requirements of the RAM are modest, especially when compared to that of other transport enhancement devices (e.g. static mixing elements, twisted ribbon, etc.) within a cylindrical geometry for highly viscous fluids. The increase in the non-Newtonian case is very modest considering the yield stress nature of this fluid. Conversely, the lengthscale of scalar transport enhancement (q_{max}) is very high in both cases – almost sixfold in the Newtonian fluid, and over threefold for the non-Newtonian fluid. For both the tube and RAM, power consumption scales with device length, so the total power required to achieve the same level of scalar transport is reduced in the RAM. These figures are reflected as P_{rel}, where 79.9% and 58.4% for the Newtonian and non-Newtonian fluid reductions in total energy consumption are achieved in the RAM for the same level of scalar transport. Whilst the operating costs of transport devices scales with energy consumption, the fixed costs scale roughly with device length, as quantified by q_{max} in Table 1.

7. Conclusions

Chaotic advection promises to enhance heat and/or mass transfer within highly viscous or rheologically complex fluids, however, optimisation is critical to realise these benefits. In this study, we applied a novel spectral method [8] to quantify asymptotic scalar transport (i.e. heat and/or mass transfer) within both Newtonian and non-Newtonian fluids over the control parameter space of a chaotic flow, the Rotated Arc Mixer (RAM). The non-Newtonian fluid under consideration is a yield stress shear thinning fluid, which is traditionally problematic for transport enhancement due to the existence of plug flow regions. A generic metric for scalar transport enhancement q is defined as the lengthscale ratio of asymptotic scalar transport in the RAM against that for a straight tube, which is universal for a variety of transport modes (homogenisation of initial conditions, boundary and domain sources). The distribution of q over the control parameter space is complex (fractal), necessitating high resolution of $\mathcal{D}$ to identify the global optimum, and study the global structure of transport in this system.

When optimised, the RAM acts as an efficient transport device for both non-Newtonian and highly viscous Newtonian fluids. At the moderate Peclét number $Pe = 10^3$, the asymptotic transport

rate increases against the reference by $q_{max} = 5.814$ and $q_{max} = 3.347$, respectively, for the Newtonian and non-Newtonian fluids, corresponding directly to a reduction in device length of q_{max} to achieve the same scalar transport. These results are universal for the Newtonian case in the Stokes regime, whereas for the non-Newtonian fluid they are general for all cases where the dimensionless RAM cell velocity $\mathbf{v}$ is constant. Furthermore, the improvements in scalar transport increase monotonically with Pe (although the optimisation process may need to be repeated). Although there exists a practical upper limit of $Pe_{max} \approx 50Pr$ based upon the fluid Prandtl number, this is expected to be $\mathcal{O}(10^5-10^7)$ for highly viscous materials. These improvements in transport come at a cost of increased energy consumption, however, this is moderate (+17% and +40%, respectively) for both the Newtonian and non-Newtonian fluids. In contrast, static and in-line mixers involve far higher relative energy consumption for laminar Newtonian flow (+500% [1] and +3600% [20], respectively), which increases further for rheologically complex materials, and the transport characteristics of these devices has been shown [11] to be similar or worse than that of the optimised RAM.

The results herein demonstrate the ability of chaotic advection to address difficult transport problems involving non-Newtonian and highly viscous fluids and indicate prospects for design and construction of low energy transport enhancement devices. In such applications optimisation of the control parameters is of paramount importance; this is facilitated by the so-called composite spectral method [8]. Although there exist a wide number [13,21] of experimental and industrial low Reynolds number transport enhancement devices based upon chaotic advection, the vast majority of these do not have a large tunable parameter space for optimisation, or they have not been globally and robustly optimised over this space. In this study, it is the combination of a number of tunable control parameters with high-resolution global exploration of the associated parameter space $\mathcal{Q}$ which facilitates exploitation of the potential of chaotic advection at the industrial scale.

References

[1] O. Byrde, M.L. Sawley, Parallel computation and analysis of the flow in a static mixer, Comput. Fluids 28 (1999) 1–18.
[2] V. Ganesan, M.D. Bryden, H. Brenner, Chaotic heat transfer enhancement in rotating annular flow systems, Phys. Fluids 9 (5) (1997) 1296–1306.
[3] J.A. Glazier, A. Libchaber, Quasi-periodicity and dynamical systems: an experimentalists view, IEEE Trans. Circuit Syst. 35 (7) (1988) 790–809.
[4] P.H. Haynes, J. Vanneste, What controls the decay of passive scalars in smooth flows?, Phys Fluids 17 (2005) 097103-1–097103-16.
[5] T.-Y. Hwu, D.-L. Young, Y.-Y. Chen, Chaotic advections for stokes flow in circular cavity, J. Eng. Mech. 123 (8) (1997) 774–782.
[6] A. Lefèvre, J.P.B. Mota, A.J.S. Rodrigo, E. Saatjian, Chaotic advection and heat transfer enhancement in Stokes flow, Int. J. Heat Fluid Flow 24 (2003) 310–321.
[7] D.R. Lester, G. Metcalfe, M. Rudman, Prospects for efficient heat transfer in an open chaotic flow, in: 13th International Heat Transaction Conference, Sydney, Australia, 2006.
[8] D.R. Lester, G. Metcalfe, M. Rudman, H. Blackburn, Global parametric solutions of scalar transport, J. Comput. Phys. (2007), doi:10.1016/j.jcp.2007.10.015.
[9] W. Liu, G. Haller, Strange eigenmodes and decay of variance in the mixing of diffusive tracers, Physica D 188 (2004) 1–39.
[10] W. Magnus, On the exponential solution of differential equations for a linear operator, Commun. Pure Appl. Math. 7 (1954) 649–654.
[11] G. Metcalfe, M. Rudman, A. Brydon, L.J.W. Graham, R. Hamilton, Composing chaos: an experimental and numerical study of an open duct mixing flow, AIChE J. 52 (2006) 9–28.
[12] J.M. Ottino, The Kinematics of Mixing: Stretching, Chaos and Transport, Cambridge University Press, Cambridge, 1989.
[13] J.M. Ottino, G. Metcalfe, S.C. Jana, Experimental studies of chaotic mixing, in: W. Ditto, L. Pecora, M. Shleshinger, M. Spano, S. Vohra (Eds.), Proceedings of the Second Experimental Chaos Conference, Office of Naval Research, 1995.
[14] A.J.S. Rodrigo, J.P.B. Mota, A. Lefèvre, E. Saatdjian, On the optimization of mixing protocol in a certain class of three-dimensional Stokes flows, Phys. Fluids 15 (6) (2003) 1505–1516.
[15] G. Rosengarten, J.J. Cooper-White, G. Metcalfe, Contact angle effects on convective heat transfer coefficient in microchannels, Int. J. Heat Mass Transfer (2007).
[16] E. Saatdjian, N. Midoux, M.I. Gastou-Chassiang, J.C. Leprevost, J.C. André, Chaotic mixing and heat transfer between confocal ellipses: experimental and numerical results, Phys. Fluids 8 (3) (1996) 677–691.
[17] P.J. Schneider, Effects of axial fluid conduction on heat transfer in the entrance region of parallel plates and tubes, Trans. ASME 79 (1957) 765–773.
[18] R. Siegel, E.M. Sparrow, T.M. Hallman, Steady laminar heat transfer in a circular tube with prescribed wall heat flux, Appl. Sci. Res. (1958) 386–392.
[19] M. Speetjens, G. Metcalfe, M. Rudman, Topological mixing study of non-Newtonian duct flows, Phys. Fluids 18 (2006) 103103-1–103103-11.
[20] F.A. Streiff, S. Jaffer, G. Schneider, The design and application of static mixer technology, in: ISMIP3, Osaka, 1999, pp. 107–114.
[21] A.D. Stroock, G.J. McGraw, Investigation of the staggered Herringbone mixer with a simple analytical model, in: J.M. Ottino, S. Wiggins (Eds.), Transport and Mixing at the Microscale, Philisophical Transactions of The Royal Society of London, 2004.
[22] Y.-K. Tsang Jr., T.M. Antonsen, E. Ott, Exponential decay of chaotically advected passive scalars in the zero diffusivity limit, Phys. Rev. E 71 (6) (2005) 1–11.